E-proceedings of the 36th IAHR World Congress
28 June – 3 July, 2015, The Hague, the Netherlands

HYDRO-MORPHODYNAMIC DIFFERENCES INDUCED BY DIFFERENT ANGLES IN AN EXPERIMENTAL DISCORDANT CONFLUENCE

SEBASTIAN GUILLÉN-LUDEÑA[1] [2]

[1] Laboratory of Hydraulic Constructions (LCH), EPFL, Lausanne, Switzerland,
sebastian.ludena@epfl.ch

[2] Instituto Superior Técnico (IST), Universidade de Lisboa, Lisbon, Portugal,
sebastian.ludena@ist.utl.pt

ABSTRACT

Confluences, within the fluvial network, are considered particular areas with great ecological value, where flow dynamics and bed morphology are complex and highly three-dimensional. Several parameters influence the morphodynamics and hydrodynamics of river confluences including discharge and momentum ratios, angle of confluence and sediment transport. Confluences with low discharge and momentum ratios, where narrow steep tributaries with high sediment load join a wide low-gradient main-channel that provides the dominant discharge, are often observed in the Upper-Rhone river in Switzerland. Few existing studies have looked at the hydro-morphodynamics of this type of river confluences considering sediment discharge in both confluent channels. This paper aims to analyze the influence of the confluence angle on the flow dynamics and bed morphology of this type of confluences in an experimental facility under movable bed conditions. For that purpose, two experiments were carried out in a laboratory confluence with low discharge and momentum ratios (Q_r = 0.11 and M_r = 0.16 respectively), and with two different confluence angles (α = 90° and 70°). During the experiments, two distinct poorly shorted sediment mixtures were supplied into the tributary and into the main channel at constant but different rates for each flume. The experiments were run until equilibrium in bed morphology was reached. During the experiments bed topography surveys were systematically recorded, and water surface was measured at equilibrium. These measures illustrate the bed topography evolution during the experiments, and the confluence hydrodynamics at equilibrium. The results show that different confluence angles resulted in different flow regimes and bed elevations in the tributary. Also, the distinct angle configurations yielded different water surface elevations in the main channel upstream of the confluence.

Keywords: *river confluences, confluence angle, discordant bed, sediment transport, supercritical flow*

1. INTRODUCTION

River confluences are systems characterized by complex morphodynamic patterns, where flow dynamics and the bed morphology closely interact to accommodate changes in flow and sediment transport that therein occur. These singularities are considered environmental hot spots within the fluvial network, contributing to the river ecosystem by providing ecological connectivity and high heterogeneity in flow (Benda et al., 2004). Confluences play also a major role in the viability of the fluvial transportation grids and it is through the confluence of tributary creeks into main rivers that the main affluences of liquid discharge and sediments are provided to the main rivers.

Among the most significant studies concerning confluence morphodynamics are those of Best (1988), Best & Rhoads (2008), and Leite Ribeiro et al. (2012a), which describe the main morphological features by means of conceptual models based on experimental tests, and those of Biron et al. (1993), Rhoads & Kenworthy (1995), Leclair & Roy (1997), Rhoads & Kenworthy (1998), Rhoads & Sukhodolov (2001), Biron et al. (2002), Boyer et al. (2006), and Rhoads et al. (2009), carried out on natural confluences.

These studies provide very valuable insights on the overall understanding of confluence morphodynamics, but few of them (Leite Ribeiro et al., 2012a; Leite Ribeiro et al., 2012b; Guillen-Ludeña et al., 2015) look at the particular characteristics found in the Upper-Rhone river confluences. In these confluences, the main stream provides the dominant discharge and the sediment are predominantly and abundantly supplied by the tributaries, whose bed level is higher than the bed of the main channel (bed discordance). Tributaries are narrower but steeper than the main stream, and such steep slopes and sediment loads often result in supercritical flows in the tributaries. The sediment provided by the tributaries is coarser than that supplied by the main stream and in both cases consists of poorly sorted gravel with high gradation coefficients. This type of confluences is characterized by low discharge and momentum ratios, which are herein defined as $Q_r = Q_{trib} / Q_{main}$ *and* $M_r = (\rho QU)_{trib} / (\rho QU)_{main}$ respectively.

This paper aims to study the differences induced by the confluence angle in the hydro-morphodynamics of an experimental confluence with low discharge and momentum ratios (Q_r = 0.11 and M_r = 0.16), where a narrow steep tributary intersects a wider nearly flat main channel at two different angles (α = 90° and α = 70°). Sediments are supplied both in the tributary and the main channel during the experiment. Systematical bed topography and water surface surveys illustrate the evolution of the bed morphology during the experiment, and the hydrodynamic features at equilibrium. The results reveal that the confluence angle (α) is determinant for the confluence morphodynamics, which are characterized by

a close interaction between the bed morphology and flow dynamics. Although inspired by the Upper-Rhone River confluences, the results herein shown and discussed may be applied to other confluences with similar physical conditions.

2. EXPERIMENTAL SET-UP AND PROCEDURE

2.1 Experimental facility

The laboratory confluence consisted of an 8.5 m long and 0.5 m wide rectangular glass flume, which corresponded to the main channel; and a tributary formed of a 4.9 m long and 0.15 m wide rectangular PVC-channel (see Figure 1). The tributary joined the main channel at two different angles: α = 90º and α = 70º. The tributary flume intersected the main channel at a distance of 3.60 and 4.00 m from the inlet for α = 90º and 70º respectively (see Figure 1).

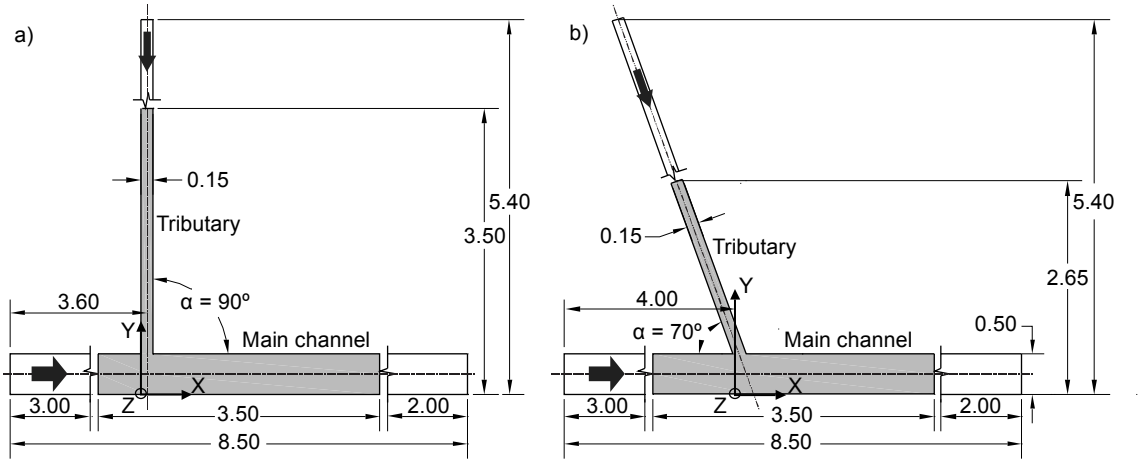

Figure 1. Plan view of the laboratory confluence. a) α = 90º, and b) α = 70º. The grey areas represent the measurement domains.

2.2 Experimental parameters

In this study, the adopted discharge ratio (Q_r = 0.11) is representative of the ratios observed in the Upper-Rhone River confluences. At the post-confluence, the flow discharge was kept constant $Q_{p\text{-}c} = Q_t + Q_m$ = 30 l/s for both confluence angles.

Two types of sediment were independently supplied during the experiments at the inlet of both channels. For the tributary, a poorly sorted mixture composed of 80% of 0.1 - 4.0 mm sand-gravel mixture, and 20% of 4.0 - 8.0 mm gravel was supplied. For the main channel, the mixture was composed of the 0.1 - 4.0 mm sand-gravel mixture supplied into the tributary, which means that the coarser part of the tributary mixture (4.0 – 8.0 mm gravel) was removed to reproduce the grain size distribution (GSD) relationship between main channel and tributary observed at the Upper-Rhone river in Switzerland. The gradation coefficient σ, defined as $\sigma = 0.5 \times (d_{84}/d_{50} + d_{50}/d_{16})$, was 4.15 for the tributary and 3.50 for the main channel. The density (ρ) and the characteristic grain diameters (d_x) of the supplied sediments are detailed in Table 1, and the GSDs are depicted in Figure 2.

Table 1. Main characteristics of the supplied sediments.

Channel	ρ_s [kg/m³]	d_{30} [mm]	d_{50} [mm]	d_{65} [mm]	d_{90} [mm]
Main channel	2650	0.4	0.8	1.4	3.0
Tributary	2650	0.4	0.8	2.3	5.7

The sediment discharges for the tributary (Q_{st}) and main channel (Q_{sm}) were defined by assuming, as initial hypothesis, that the longitudinal bed slope and GSDs were in the range of those observed in the Upper-Rhone river confluences. Hence, the hypothetical bed slopes under equilibrium conditions were assumed to be 1.0% for the tributary and within the range of 0.3% – 0.4% for the main channel. By assuming uniform flow in both channels for such slopes and for the adopted discharge ratio, the sediment discharges for both channels were obtained through the formula of sediment transport in gravel bed rivers of Smart & Jaeggi (1983) and Smart (1984) Eq [1].

$$Q_b = B_F \times \rho_s \times \frac{4}{s-1} \times R_h \times U \times J^{0.6} \times \left(J - \frac{d_{65}}{12.1 \times R_h}\right) \times \left(\frac{d_{90}}{d_{30}}\right)^{0.2} \quad [1]$$

where Q_b is the sediment transport rate (bed load), B_F is the width of the flume, ρ_s is the sediment density (2650 kg/m³), s is the relative sediment density (ρ_s/ρ = 2.65), ρ is the water density (ρ = 1000 kg/m³), R_h is the hydraulic radio, U is the mean water velocity, J is the slope of the channel bed, and d_{65}, d_{90}, and d_{30} are characteristic grain diameters obtained from Table 1 and Figure 2. The values obtained for sediment discharges for both experiments were 0.3 kg/min for the main channel (Q_{sm}) and 0.5 kg/min for the tributary (Q_{st}).

The downstream flow depth (y_d) in the main channel was controlled by means of an adjustable tail-gate. As the flow and sediment discharges at the post-confluence coincided for both confluence angles, the value of y_d was kept constant for both experiments. This flow depth (y_d) was defined by assuming uniform flow in the post-confluence, and it was computed through the Manning-Strickler formula. For this computation, the flow discharge at the post-confluence was $Q_{p\,c}$ = 30 l/s, the bed slope J_b = 0.4%, and the Strickler friction coefficient K_{st} = 78 $m^{1/3}s^{-1}$ approached as $K_{st} = 26/(d_{65})^{1/6}$, with d_{65} = 1.4 mm. The adopted downstream flow depth was y_d = 0.08 m. This value (y_d = 0.08 m) and the value of the main channel width (B = 0.50 m) are used in this study to normalize the variables.

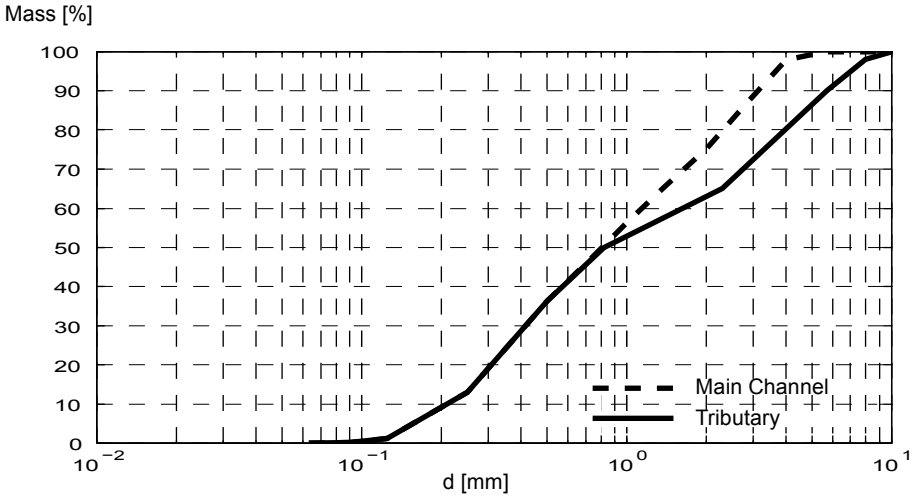

Figure 2. Grain size distribution (GSD) for supplied sediments into tributary and main channel

2.3 Experimental procedure and measurements

Before each experiment, the initial bed was prepared using the same sediment mixtures that subsequently were supplied into each channel, (cf. Table 1 & Figure 2). To accelerate the morphology evolution in the tributary, a small bed discordance of roughly 0.03 m was imposed at the tributary mouth, together with a bed slope of about 0.5%. This initial bed morphology did not affect to the final one since, as verified later, the initial slope and the initial bed discordance resulted smaller than those reached in equilibrium.

Once the channel beds were prepared, the model was slowly filled with water, and bed topography was recorded in both flumes before the beginning of the experiments (t = 0 h). Later, topographic surveys were taken after one hour (t = 1 h), at seven hours (t = 7 h), and at equilibrium, which was reached after 14 hours for α = 90° (t = 14 h), and after 16 hours for α = 70° (t =16 h).

Bed topography was measured with a Mini-Echo-Sounder with ± 1mm of accuracy, whereas for the water surface an ultrasonic limnimeter with an accuracy of ± 1 mm was used. Both measurements consisted of nine longitudinal profiles, laterally spaced by ΔY = 0.05 m (Y = 0.05 to 0.45 m), with a spatial resolution of ΔX = 0.01 m, along the main channel, and one profile along the tributary axis.

To determine when the tests attained equilibrium, the sediment transport at the downstream end was evaluated by weighting the outgoing sediments, after 1, 5, 10, 11, 12, 14 and 15 hours. Additionally, equilibrium was also checked by measuring the channel bed level evolution at five different control points after 1, 7, 10, 12, 13, 14 and 15 hours. When the outgoing sediment discharge was equal or larger than 90% of the incoming, and the rate of change of the bed elevation ($r(t_i) = 100\ |Z(t_i) - Z(t_i\text{-}1)| \ / \ Z(t_i\text{-}1)$) represented less than 2% for the five control points, the test was considered in equilibrium and stopped.

3. RESULTS

3.1 Bed morphology evolution

At the beginning of the experiments (t = 0 h), the main channel presented fairly flat bed for both confluence angles. In the tributary, at t = 0h, the bed topography presented a slight slope and a small imposed discordance at the junction with the main channel (Figure 3a&b).

During the first hour of the experiments (t = 1 h), a scour hole formed at the tributary mouth for both confluence angles (Figure 3c-d & Figure 4a-b). These scour holes were excavated in the bed of the main-channel by the turbulence associated to the flow junction. For α = 90° the maximum depth of the scour hole was Z = -0.041 m, whereas for α = 70° it was Z = -0.027 (Figures 3c-d & 4a-b). For α = 90° a deposition formed by the eroded material was observed at the inner bank of the main channel, downstream of the confluence (Figures 3c & 4a).

In the tributary, at t = 1 h, a sediment-wave front was identified at Y/B = 2 for α = 90° (Figures 3c & 4e). This wave was formed by the supplied sediment, and it gradually progressed downstream by raising the bed level (Figure 4e). In contrast, for α = 70°, the tributary bed did not present any significant variation with respect to the initial bed (Figures 3d & 4f).

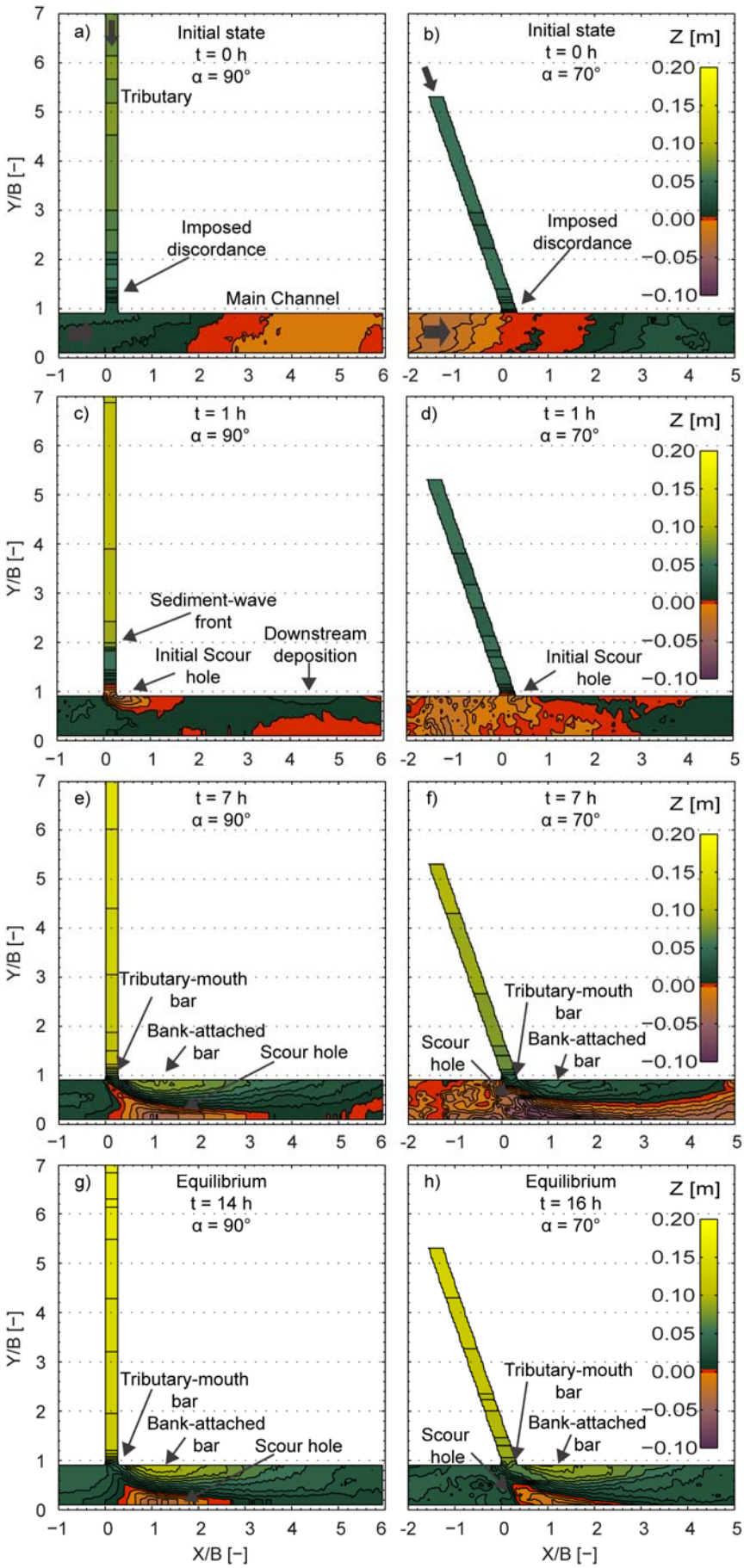

Figure 3. Bed topography evolution with contours spaced ΔZ = 0.01 m. a) α = 90°, t = 0 h; b) α = 70°, t = 0 h; c) α = 90°, t = 1 h; d) α = 70°, t = 1 h; e) α = 90°, t = 7 h; f) α = 70°, t = 7 h; g) α = 90°, t = 14 h; h) α = 70°, t = 16 h

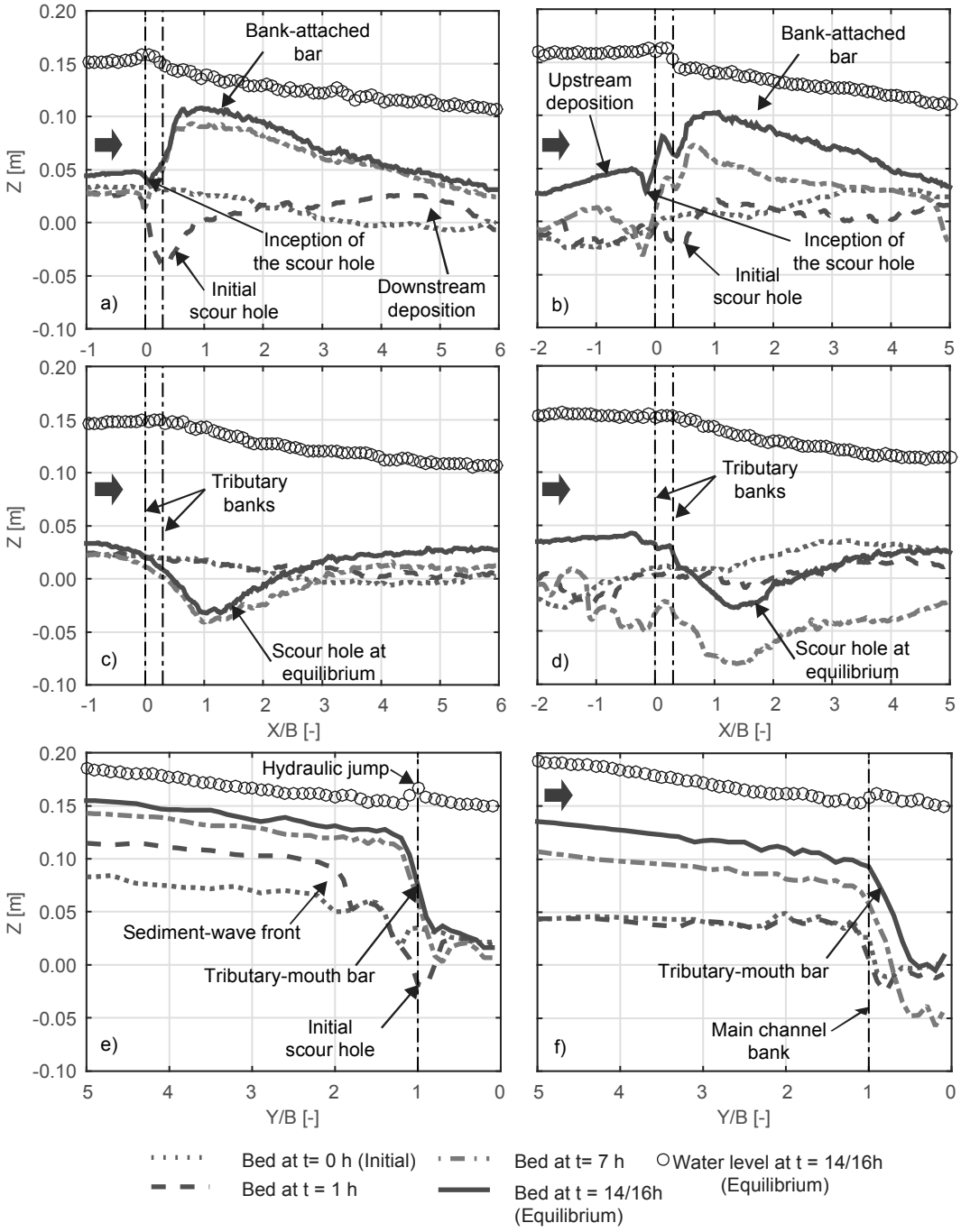

Figure 4. Longitudinal profiles of the bed and water surface evolution at the inner bank of the main channel: a) α = 90°; b) α = 70°; at the outer bank of the main channel: c) α = 90°; c) α = 70°; and at the tributary axis: e) α = 90°; f) α = 70°.

For both confluence angles, the sediment coming from the tributary in the form of a migrating sediment-wave filled progressively the scour hole and deposited in the main channel, where a bar along the inner bank was formed. These bars are widely termed as “bank-attached bars” (Best & Rhoads, 2008). At t = 7 h, both experiments presented well-developed bars in the main channel (Figures 3e-f & 4a-b). These bars reduce the effective flow-section in the main channel and confine the flow to the outer bank, leading to flow acceleration and bed erosion therein (Figures 3e-f & 4a-d).

In both experiments, after 7 hours, the tributary attained a quasi-equilibrium bed morphology consisting of a steep bed slope, a raised bed elevation and well-developed bed discordance with the main channel (Figures 3e-f & 4e-f). The transition between tributary and main channel was characterized by an abrupt slope or avalanche face that penetrated further for α = 70° than for α = 90° into the main channel. This feature is termed as “tributary-mouth bar” (Best & Rhoads, 2008).

From 7 hours to equilibrium, the bed topography for α = 90° only experienced minor changes including a small increase in the height of the bank-attached bar and in the bed elevation of the tributary (Figure 4a, c & e). For α = 70°, the bed morphology evolution from 7 hours to equilibrium consisted in a major increase of the bed elevation of about 0.05 m in the main channel and of about 0.02 m in the tributary (Figure 4b, d & f).

At equilibrium, both experiments presented similar bed morphologies consisting of: i) a scour hole which started at the tributary mouth and bisected the junction angle until reaching the outer bank, where it became parallel to the lateral banks; ii) a bar attached to the inner bank of the main channel (bank-attached bar), formed by the sediment coming from the tributary; iii) a marked bed discordance between the main-channel and the tributary bed levels; and iv) a steep bed slope in the tributary which remains constant until reaching the confluence.

Some morphological differences were also observed at equilibrium for the distinct confluence angles, these consisted of: i) a deposition at the inner bank of the main channel, upstream of the confluence for α = 70° and not observed for α = 90° (cf. Figure 4b); ii) a further penetration of the tributary bed into the main channel for α = 70° (cf. Figure 4e-f); and iii) the inception of the scour hole, which was observed at the inner bank of the main channel further upstream for α = 70° (X/B < 0) than for α = 90° (X/B > 0) (cf. Figure 4a-b).

3.2 Hydrodynamics at equilibrium

In both experiments, at the inner bank of the main channel, the water level profiles exhibited an upstream oriented slope (cf. Figure 4a-b). These profiles correspond to a M1-type backwater curve (Chow, 1959) induced by the tributary inflow. At the upstream junction corner, for α = 90°, the water surface reached a maximum (Z = 0.160 m), whereas for α = 70° the maximum (Z = 0.162 m) was reached within the junction (0.0 < X/B < 0.3). These local increases of the water level may be associated to a zone of stagnation caused by the flow junction. At the downstream junction corner (X/B = 0.3), both experiments presented a drop in the water surface revealing a low-pressure zone. Associated to these low-pressure zones, flow upwelling was also observed at the downstream junction corner of each experiment (cf. Figure 5). Downstream of this (X/B > 0.3), the water surface slope became steeper indicating flow acceleration (cf. Figure 4a-b).

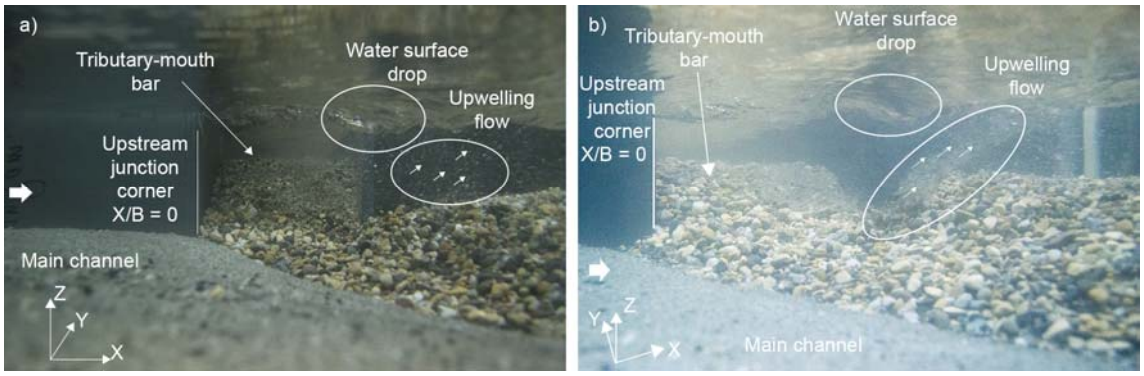

Figure 5. Frontal view of the tributary mouth for a) α = 90°; and b) α = 70°. Notice the flow upwelling at the downstream junction corner

At the outer bank of the main channel, the water surface presented low-gradient profiles in the region upstream of the confluence for both confluence angles (cf. Figure 4c-d). These water level profiles also correspond to M1-type backwater curves (Chow, 1959), which was induced by the tributary inflow. Downstream of the confluence, the slope of the water level profiles at the outer bank increased due to the flow acceleration observed therein (cf. Figure 4c-d).

In the tributary, for α = 90°, the water surface at equilibrium showed a steep and nearly constant slope until reaching the confluence (cf. Figure 4e). At the mouth (Y/B = 1 in Figure 4e), an abrupt increase in water surface elevation revealed the presence of a hydraulic jump, as the tributary flow upstream of the confluence was supercritical (Fr > 1). Furthermore, in the tributary at equilibrium, the water level profile was parallel to the bed, indicating that the flow was nearly uniform.

For α = 70°, the water level profile in the tributary presented a steep slope upstream of the confluence (cf. Figure 4f). Also, a local increase in water surface elevation due to the flow junction was observed at the confluence (Y/B = 1 in Figure 4f). In this case, the flow was sub-critical (Fr < 1) contrasting with α = 90°.

Figure 6 depicts the cross-sectional average (CSA) profiles of bed elevation, water level and total energy (H) for the main channel and tributary at equilibrium for both confluence angles. The total energy profile was computed as in Eq. [2] by using the CSA values of bed elevation (Z), water depth (y) and flow velocity (U). The pressure distribution was assumed to be hydrostatic, and the cross-sectional velocity distribution was assumed to be uniform.

$$H = Z + y + \frac{U^2}{2 * g} \qquad [2]$$

where g is the acceleration of gravity

In the main channel, the CSA bed elevation profiles are similar for both confluence angles, illustrating the scour hole at the confluence and the bar formed downstream (cf. Figure 6a). The CSA water level profiles present different elevations for X/B < 1, where the water level corresponding to α = 90° is lower than that corresponding to α = 70° (cf. Figure 6a). For X/B > 1 both profiles converge and become parallel to each other. The total energy profiles present a first reach nearly horizontal upstream of the confluence (X/B < 0 in Figure 6a). These low-gradient profiles correspond to a decrease in the kinetic energy component of the main flow in benefit of the potential energy, which is manifested by the raising of the piezometric height, herein considered as the flow depth. At the downstream junction corner (X/B ≈ 0.3 in Figure 6a), both energy profiles (α = 90° and 70°) present a drop indicating the local energy loss caused by the tributary inflow, which was higher for α = 70° than for α = 90°. Farther downstream, there is a transition in which the slope of the energy profiles

gradually increases reflecting the flow acceleration experienced by the main channel flow. The length of this transition varies for the different angle configurations, for α = 90° it was observed for 0.3 < X/B < 3.0, whereas for α = 70° it was shorter, for 0.3 < X/B < 2.0 (cf. Figure 6a). Downstream of this transition, the energy slope (J_E) becomes constant and parallel to the bed slope (J_b), revealing that the flow was quasi uniform for X/B > 3.0 for α = 90°, and for X/B > 2.0 in the case of α = 70°.

In the tributary, the total energy profiles present some differences between the distinct confluence angles. For α = 90°, the kinetic component is larger than for α = 70° (cf. Figure 6b). This difference is due to the lower flow depth and higher flow velocity registered for α =90°. Also, for α = 90°, the energy slope (J_E) upstream of the confluence (Y/B > 1.5) is parallel to the bed slope (J_b) revealing that the flow was quasi uniform (cf. Figure 6b). In contrast, for α = 70° the energy slope (J_E) upstream of the confluence (Y/B) is steeper than the bed slope (J_b).

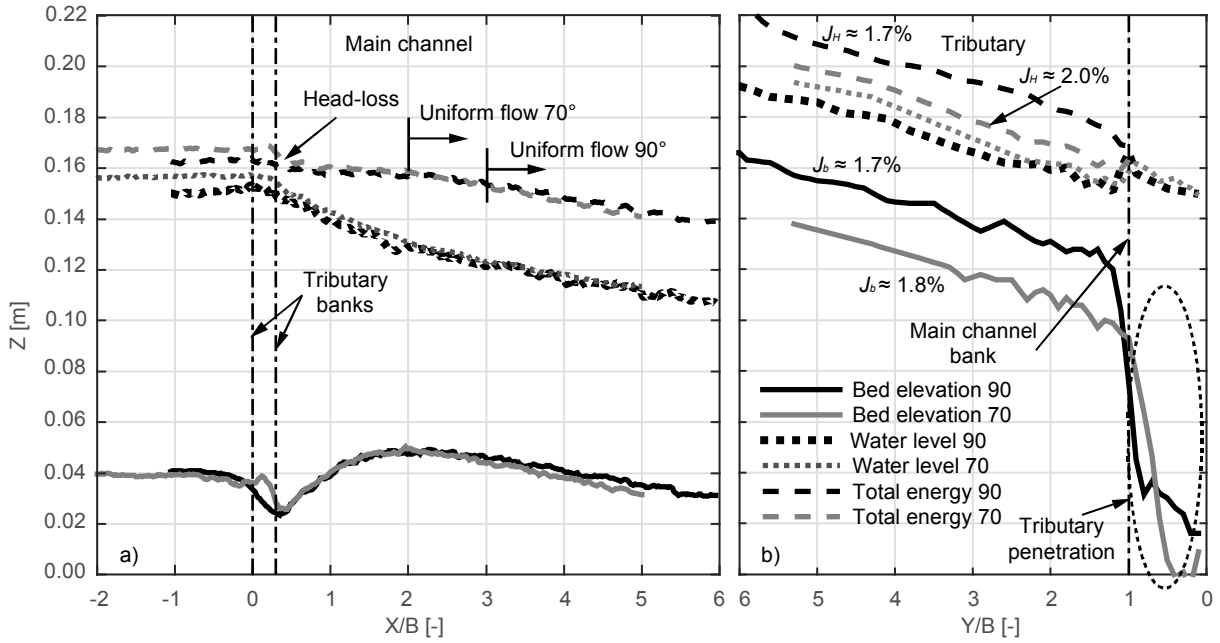

Figure 6. Cross-sectional average profiles of bed elevation, water level and total energy at equilibrium for both confluence angles, a) at the main channel; and b) at the tributary axis

To determine the different flow regimes observed in the tributary and main channel at equilibrium, the Froude number was computed by considering the CSA values of flow depth (y) and flow velocity (U) along the tributary and main channel (see Figure 7). For both angle configurations, the flow regime in the main channel at equilibrium was sub-critical (Fr < 1) all along the flume (cf. Figure 7a). Upstream of the confluence (X/B < 0), the main flow presents low Froude values in both angle configurations (cf. Figure 7a), which is coherent with the low-gradient profiles of water level and energy observed in the same zone (cf. Figure 6a). For 0 < X/B < 3 in the case of α = 90°, the Froude values increase reflecting the flow acceleration experienced by the main flow (cf. Figure 7a). The same pattern is observed for α = 70° but in a shorter length, i.e. for 0 < X/B < 2 (cf. Figure 7a). For X/B > 3 in the case of α = 90°, and for X/B > 2 for α = 70°, the Froude values become nearly constant indicating a constant flow velocity (cf. Figure 7a).

In the tributary, the flow at equilibrium presents different flow regimes for each angle configuration. For α = 90°, the flow was supercritical (Fr > 1) upstream of the confluence (Y/B > 1.5), whereas for α = 70°, for Y/B > 1.5, the flow was sub-critical (Fr < 1) (cf. Figure 7b).

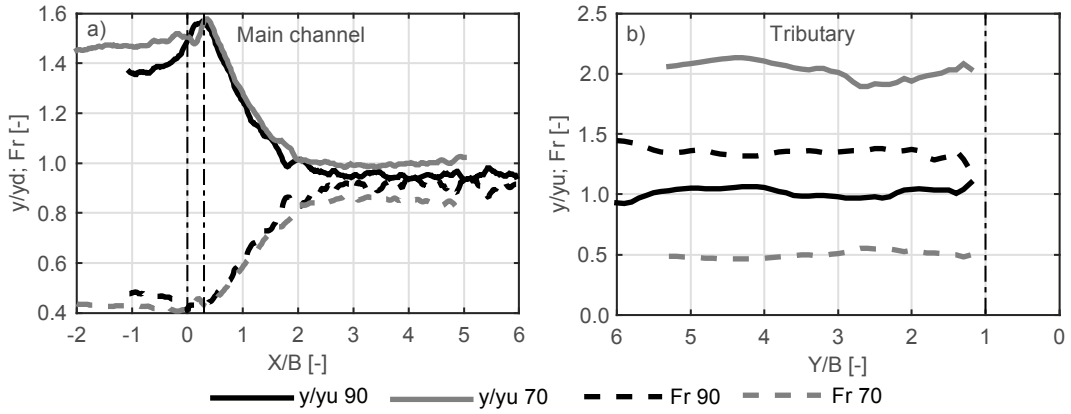

Figure 7. Cross-sectional average profiles of the dimensionless flow depth (y/y_u) and Froude number at equilibrium for both angle configurations. a) at the main channel; and b) at the tributary

Figure 7 also depicts the values of the CSA flow depth (y) along the main channel and tributary for both angle configurations. For the main channel, the flow depth (y) values were nomalized by the flow-depth imposed at the downstream end of the main channel (y_d). This value is considered as a reference for both angle configurations, since it represents the downstream boundary condition of the confluence system initially established, and it was the same in both experiments.

For the main channel, upstream of the confluence (X/B < 0), the flow-depth for α = 90° was lower than for α = 70°, indicating higher flow velocities for the right angle (cf. Figure 7a). Within the junction (0.0 < X/B < 0.3), the flow depth increased for both angle configurations due to the reported water level increase and the bed erosion in this region (cf. Figure 7a). Downstream of the confluence, the flow-depth decreases until reaching a value close to y_d ($y/y_d \approx 1$). This point is about X/B = 3 for α = 90° and about X/B = 2 for α = 70° (cf. Figure 7a). Downstream of this, the flow depth remains nearly constant for both angles, indicating that the flow was quasi-uniform (cf. Figure 7a).

In the tributary, the flow-depth at equilibrium was normalized by the uniform flow depth (y_u = 0.028 m). This value was obtained through the Manning-Strickler formula, by considering the flow discharge in the tributary (Q_t), the bed slope (J_b), and the Strickler's friction coefficient approached as $K_{st} = 26 / (d_{65})^{1/6}$, where d_{65} is the characteristic grain diameter of the sediment mixture supplied into the tributary (d_{65} = 2.3 10^{-3} m). As the bed slope was fairly the same for both angle configurations (cf. Figure 6c-d), the adopted value was J_b = 1.7%. Table 2 contains the values of the flow discharge (Q_t), channel width (B), bed slope (J_b), energy slope (J_E), flow depth (y), critical-flow depth (y_c), mean flow velocity (U), Froude number, characteristic grain diameter (d_{65}), and Strickler's friction coefficient (K_{st}) for the tributary at equilibrium for both angle configurations.

Table 2. Hydraulic variables of the tributary at equilibrium for both angle configurations

	Q_t	B	J_b	J_E	y	y_c	y_u	U	Fr	d_{65}	K_{st}
[°]	[l/s]	[m]	[%]	[%]	[m]	[m]	[m]	[m/s]	[-]	[mm]	[$m^{1/3}s^{-1}$]
90	3.0	0.15	1.7%	1.7%	0.028	0.034	0.028	0.71	1.36	2.30	72
70			1.8%	2.0%	0.055			0.36	0.50		

From Figure 7b and Table 2, it is possible to infer that for α = 90° the flow was nearly uniform upstream of the confluence; whereas for α = 70°, the flow at equilibrium was far from uniform as depicted in Figure 7b. Moreover, for α = 70°at equilibrium, the flow depth (y) was larger than the critical and the uniform flow depths (y_c and y_u respectively in Table 2), which reveals that the flow at equilibrium corresponds to a spatially varied flow with steep bed slope.

4. DISCUSSION

4.1 Morphological differences induced by the confluence angle

The results presented in this study clearly showed that the evolution of the bed morphology and the morphological features at equilibrium change with the confluence angle.

The scour hole observed at the tributary mouth after the first hour of the experiments (t = 1h) is considerably deeper for α = 90º than for α = 70º (cf. Figure 3c-d and Figure 4a-b). This difference indicates that the lower angle (α = 70º) smoothed the effect of jet-like tributary inflow into the main-channel, compared with the right angle configuration (α = 90º). This smoothing effect observed for α = 70° may be attributed to the velocity component of the tributary parallel to the streamwise flow direction of the main channel. In the case of α = 90°, due to the perpendicular tributary inflow, the flow junction resulted in a more intense turbulent flow which eroded the bed locally. This scour hole is a typical feature observed either in symmetrical or asymmetrical concordant confluences, as reported by Mosley (1976). Similar confluence scour holes were also reported by other authors such as Ashmore & Parker (1983); Best (1988) and Ghobadian & Bajestan (2007).

For both confluence angles, the sediment coming from the tributary deposited at the downstream junction corner creating a bar along the inner bank of the main channel. This bar is widely termed as "bank-attached bar", and it is typically associated with flow separation at the downstream junction corner, though it may also form in regions of flow deceleration without actual flow separation (Best and Rhoads 2008).

At equilibrium, in the case of α = 90º, the inception of the bank-attached bar is located downstream of the confluence, separate of the tributary-mouth bar. In contrast, for α = 70º, the bank-attached bar begins at the upstream junction corner merging with the tributary-mouth bar as depicted in Figures 8 & 9. This difference was due to the further penetration of the tributary-mouth bar into the main channel for α = 70°, compared to the case of α = 90° (cf. Figure 6b).

For both confluence angles, the bank-attached bar steered the near-bed flow of the main channel towards the outer bank. In parallel, the tributary inflow deflected the near-surface flow towards the outer bank. There, both flows converged leading to a flow acceleration and bed erosion creating a scour hole.

For α = 70°, the deposition observed at equilibrium at the inner bank of the main channel upstream of the confluence (cf. Figure 4b) indicates the beginning of the near-bed flow deflection. This deposition was not observed at equilibrium for α = 90° (cf. Figure 4a) as the near-bed flow was deflected farther downstream where the bank-attached bar began (cf. Figure 4a).

The bed elevation of the tributary at equilibrium was higher for α = 90° than for α = 70°. Nevertheless, the bed discordance formed with the main-channel bed was similar for both confluence angles (cf. Figure 6b). Upstream of the confluence, for Y/B > 1.5, the bed slope in the tributary (J_b) is slightly steeper for α = 70º than for α = 90º (cf. Figure 6b & Table 2).

To convey the imposed tributary bedload, the tributary bed adopted steep bed slopes at equilibrium for both angle configurations, independently of the final flow regime observed at the experiments, which implies that the imposed sediment discharge exerted a major influence on the tributary bed slopes at equilibrium.

The angle formed between the toe of the bank-attached bars and the outer bank of the main-channel is observed to be lower for α = 90º than for α = 70º (cf. Figure 9). This indicates that, for the lower angle (α = 70º), the tributary flow penetrates into the main channel depositing the tributary bedload and deflecting the main channel flow. For α = 90º, the tributary bedload is delivered into the main channel through the tributary avalanche slope, where the resulting turbulent flow from the junction conveys this load farther downstream until being deposited in the bank-attached bar. In other words, the penetration of the tributary sediments into the main channel is facilitated, when the direction of conveyance of the bedload is better aligned with the streamwise momentum-direction in the main channel.

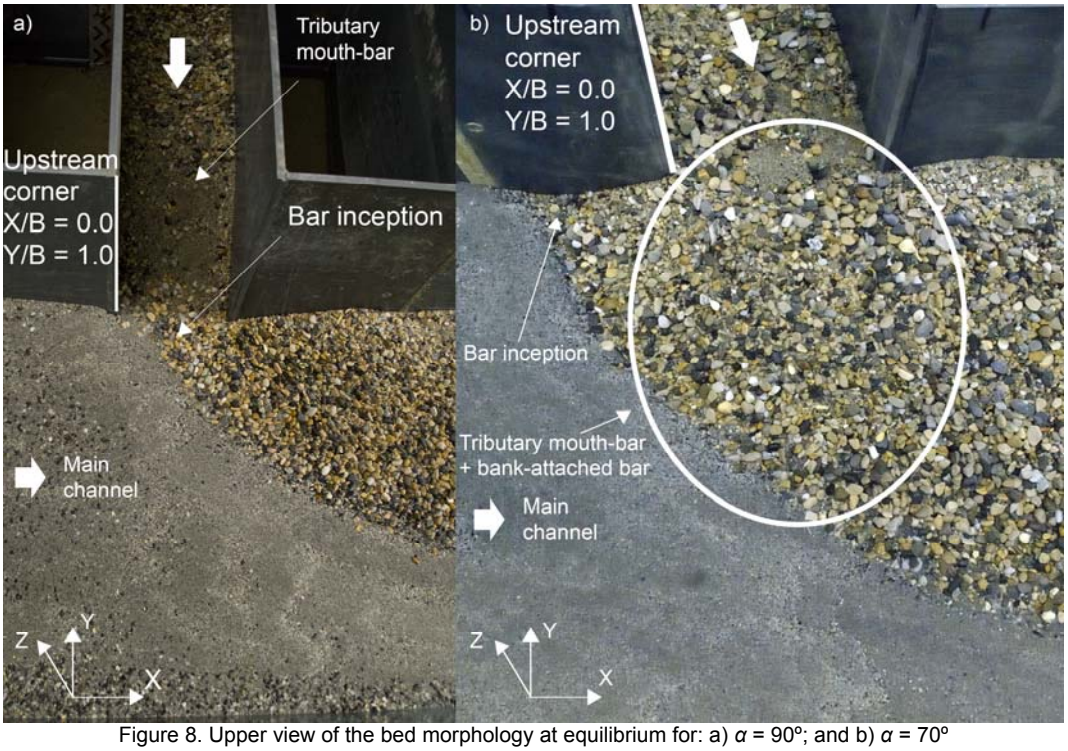

Figure 8. Upper view of the bed morphology at equilibrium for: a) α = 90º; and b) α = 70º

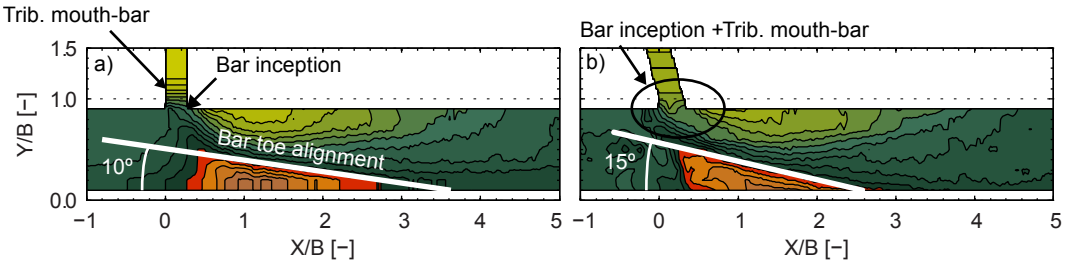

Figure 9. Detailed view of the confluence system at equilibrium for: a) α = 90º; and b) α = 70º.

4.2 Hydrodynamic differences induced by the confluence angle

4.2.1 Main channel

For α = 90°, the flow in the main channel increases the potential energy component by decreasing the kinetic one in the upstream region to overcome the jet-like tributary inflow. This is reflected in the upstream-oriented slope of the CSA water level profile upstream of the confluence (cf. Figure 6a). In the case of α = 70°, the lower angle smooths the flow junction, and the main flow does not need to gain energy by increasing the water level to overcome the tributary inflow. In this case (α = 70°), the kinetic and potential component of the total flow energy remain constant upstream of the confluence, which is reflected in a horizontal reach in the water level profile (X/B < 0 in Figure 6a).

Downstream of the confluence (X/B > 0), the flow accelerates and tends asymptotically to uniform for both confluence angles. This approach to uniform flow was shorter for α = 70° where the flow became quasi-uniform for X/B > 2, whereas for α = 90° the flow became quasi-uniform for X/B > 3 (cf. Figure 6a & Figure 7a). Such difference may be justified by the different flow regimes registered for α = 90° between the tributary (supercritical) and the main channel (sub-critical), which did not occur for α = 70°, where the flow was sub-critical in both channels. The transition from the supercritical flow in the tributary to the sub-critical flow in the main channel, through a hydraulic jump, induces a higher perturbation in the main flow for α = 90° than for α = 70°.

The total energy profiles show that for α = 70°, the head loss at the downstream corner of the confluence is higher than for α = 90°. This is coherent with the higher flow-depths register upstream of the confluence for α = 70°, in comparison to the flow depth measured for α = 90° (cf. Figures 6a & 7a). To analyzes this finding, energy and momentum balance are performed between the cross-section X/B = -1 and X/B = 5. These are the furthermost cross-section of the confluence in which data are available for both experiments.

Table 3 contains the values of momentum (M) and total energy (H) in each one of the cross-sections, which are referred by the sub-index 1 for X/B = -1 and 2 for X/B = 5. The momentum was computed as in Eq [3]:

$$M = \rho Q U + \frac{1}{2}\Upsilon y^2 B \qquad [3]$$

where ρ is the density of the water (1000 *kg/m³*), Q is the flow discharge (Q_1 = 0.027 m³/s; and Q_2 = 0.030 m³/s), U is the mean flow velocity, γ is the specific weight of water (9800 N/m³), y is the cross-sectional averaged water depth, and B is the channel width (B = 0.50 m).

Table 3. Momentum and energy values at the cross-section 1 (X/B = -1) and 2 (X/B = 5) for both confluence angles

α [°]	M_1 [N]	M_2 [N]	$M_1 - M_2$ [N]	H_1 [m]	H_2 [m]	$H_1 - H_2$ [m]
90	43	38	5	0.162	0.143	0.020
70	46	38	8	0.167	0.141	0.027

From Table 3, it is possible to infer that the momentum transferred from the tributary to the main flow was higher for α = 70° than for α = 90° $(M_1 - M_2)_{70} > (M_1 - M_2)_{90}$. This was thanks to the lower angle which enhances the alignment between the streamwise velocity components of each flume. The momentum balance also shows that between the two cross-sections analyzed, the resistance to the flow ($M_1 - M_2$) is higher for α = 70° than for α = 90°. The energy balance reveals that the head loss between the cross-section 1 and 2 is higher for α = 70° than for α = 90°. Such behavior may be due to the hydraulic jump observed at equilibrium in the tributary mouth for α = 90°. This hydraulic jump dissipates part of energy of the tributary flow before entering the main channel and thus, the tributary inflow induces a lower head loss in the main flow in comparison with the case of α = 70°, where no hydraulic jump was observed since both flows were sub-critical at equilibrium.

Other experiments performed by the author (not shown here) with different discharge ratios present coherent behaviors in terms of head losses for the different confluence angles. When the tributary flow is supercritical (Fr > 1), which occurs only for α = 90°, the head losses due to the junction in the main channel are lower than for the same discharge ratio but α = 70°, where the tributary flow is always sub-critical (Fr < 1). On the contrary, for the cases of α = 90° in which the tributary flow is sub-critical or critical (Fr ≤ 1), the head losses in the main channel for α = 90° are higher than for α = 70°.

4.2.2 Tributary

At equilibrium, the tributary presents different flow regimes for the distinct confluence angles, i.e. for α = 90° the flow was nearly uniform and supercritical (Fr > 1), whereas for α = 70° a sub-critical spatially varied flow (Fr < 1) with a steep bed slope was observed in the tributary.

For α = 90º, the tributary flow evolved to supercritical regime to convey the imposed sediment load to the main channel. This supercritical flow was attained by raising the bed elevation up to reaching the necessary flow velocity able to transport the sediment load to the main channel. For such bed level and flow depth, the main flow did not influence the tributary flow in the sense of not imposing a downstream boundary condition. In the case of α = 70°, the lower angle enhanced the alignment between the streamwise flow direction of both flumes. This better alignment eased the delivery of the tributary sediment to the main channel, and the tributary flow did not need to raise the bed level up to attaining supercritical flow to convey the sediment load into the main channel. Under these conditions of bed elevation and flow depth, the main flow imposed the downstream boundary condition to the tributary flow, which at equilibrium corresponded to a sub-critical gradually varied flow. The lower flow velocities in the tributary and the main channel upstream of the confluence for α = 70° with respect to the case of α = 90° may explain the different times to reach equilibrium observed for α = 90° (t =14 h) and for α = 70° (t =16 h).

5. CONCLUSIONS

The effects of the confluence angle on the bed morphology evolution and hydrodynamics at equilibrium were herein studied in a laboratory open-channel confluence with movable bed for two confluence angles, with low discharge and momentum ratios and with constant sediment discharge in both flumes.

The confluence angle (α) was identified as an influent parameter on the bed morphology and the hydrodynamics of the confluence. In this study, different confluence angles altered the bed morphology evolution yielding differences in the morphological features observed at equilibrium. Also, the hydrodynamics at equilibrium was affected by different angle configurations.

For α = 70°, the bed elevation of the tributary at equilibrium was lower than in the case of α = 90°. Also, for α = 70°, the tributary bed penetrated further into the main channel with respect to the case of α = 90°. The better alignment of the streamwise flow direction enhances the penetration of the tributary bed into the main channel, and this further penetration facilitates the conveyance of the tributary sediment load into the main channel.

Different flow regimes were observed in the tributary at different confluence angles. For α = 90º the tributary presented super-critical uniform flow and the transition to the sub-critical main flow was through a hydraulic jump. In the case of α = 70º the flow in the tributary was classified as sub-critical spatially varied.

In the main channel, the energy loss measured at equilibrium for α = 90° was lower than for α = 70°. Such difference may be due to the hydraulic jump registered at the tributary mouth in the case of α = 90°, which dissipated part of the flow energy of the tributary before entering the main flow. As the main channel flow was sub-critical for both confluence angles, the higher head loss at the junction observed at equilibrium for α = 70° implied higher water depths upstream of the confluence with respect to the case of α = 90°.

ACKNOWLEDGMENTS

This research was supported by the Portuguese national Funding agency for Science, research and Technology (FCT) and the Laboratory of Hydraulic Construction (LCH) at EPFL in the framework of the Joint Doctoral Initiative IST-EPFL, and of the projects SFRH/BD/51453/2011, PTDC/ECM/118775/2010, and the LCH/EPFL.

REFERENCES

Ashmore, P., & Parker, G. (1983). Confluence scour in coarse braided streams. *Water Resources Research*, *19*(2), 392–402. doi:10.1029/WR019i002p00392

Benda, L., Andras, K., Miller, D., & Bigelow, P. (2004). Confluence effects in rivers: Interactions of basin scale, network geometry, and disturbance regimes. *Water Resources Research*, *40*(5). doi:10.1029/2003WR002583

Best, J. L. (1988). Sediment transport and bed morphology at river channel confluences. *Sedimentology*, *35*(3), 481–498. doi:10.1111/j.1365-3091.1988.tb00999.x

Best, J. L., & Rhoads, B. L. (2008). Sediment transport, bed morphology and the sedimentology of river channel confluences. In S. P. Rice, A. G. Roy, & B. L. Rhoads (Eds.), *River Confluences, Tributaries and the Fluvial Network* (pp. 45–72). Chichester, UK: John Wiley & Sons, Ltd. doi:10.1002/9780470760383.ch4

Biron, P. M., Richer, A., Kirkbride, A. D., Roy, A. G., & Han, S. (2002). Spatial patterns of water surface topography at a river confluence. *Earth Surface Processes and Landforms*, *27*(9), 913–928. doi:10.1002/esp.359

Biron, P. M., Roy, A. G., Best, J. L., & Boyer, C. J. (1993). Bed morphology and sedimentology at the confluence of unequal depth channels. *Geomorphology*, *8*(2-3), 115–129. doi:10.1016/0169-555X(93)90032-W

Boyer, C., Roy, A. G., & Best, J. L. (2006). Dynamics of a river channel confluence with discordant beds: Flow turbulence, bed load sediment transport, and bed morphology. *Journal of Geophysical Research: Earth Surface*, *111*(F4), F04007. doi:10.1029/2005JF000458

Chow, V. Te. (1959). *Open-Channel Hydraulics*. New York: McGraw-Hill Book Company,Inc.

Ghobadian, R., & Bajestan, M. S. (2007). Investigation of Sediment Patterns at River Confluence. *Journal of Applied Sciences*, *7*(10), 1372–1380. doi:10.3923/jas.2007.1372.1380

Guillen-Ludeña, S., Franca, M. J., Cardoso, A. H., & Schleiss, A. J. (2015). Bed morphology and hydrodynamic evolution in a 90° discordant confluence with low discharge ratio. *Earth Surface Processes and Landforms* (under revision).

Leclair, S. F., & Roy, A. G. (1997). Variability of bed morphology and sedimentary structures at a discordant river confluence during low flows. *Geographie Physique et Quaternaire*, *51*(2), 125–139.

Leite Ribeiro, M., Blanckaert, K., Roy, A. G., & Schleiss, A. J. (2012a). Flow and sediment dynamics in channel confluences. *Journal of Geophysical Research*, *117*(F1), F01035. doi:10.1029/2011JF002171

Leite Ribeiro, M., Blanckaert, K., Roy, A. G., & Schleiss, A. J. (2012b). Hydromorphological implications of local tributary widening for river rehabilitation. *Water Resources Research*, *48*(10), n/a–n/a. doi:10.1029/2011WR011296

Mosley, M. P. (1976). An experimental study of channel confluences. *Journal of Geology*, *84*(5), 535–562. Retrieved from http://www.jstor.org/stable/30066212

Rhoads, B. L., & Kenworthy, S. T. (1995). Flow structure at an asymmetrical stream confluence. *Geomorphology*, *11*(4), 273–293. doi:10.1016/0169-555X(94)00069-4

Rhoads, B. L., & Kenworthy, S. T. (1998). Time-averaged flow structure in the central region of a stream confluence. *Earth Surface Processes and Landforms*, *23*(2), 171–191. doi:10.1002/(SICI)1096-9837(199802)23:2<171::AID-ESP842>3.0.CO;2-T

Rhoads, B. L., Riley, J. D., & Mayer, D. R. (2009). Response of bed morphology and bed material texture to hydrological conditions at an asymmetrical stream confluence. *Geomorphology*, *109*(3-4), 161–173. doi:10.1016/j.geomorph.2009.02.029

Rhoads, B. L., & Sukhodolov, A. N. (2001). Field investigation of three-dimensional flow structure at stream confluences: 1. Thermal mixing and time-averaged velocities. *Water Resources Research*, *37*(9), 2393–2410. doi:10.1029/2001WR000316

Smart, G. M. (1984). Sediment Transport Formula for Steep Channels. *Journal of Hydraulic Engineering*, *110*(3), 267–276. doi:10.1061/(ASCE)0733-9429(1984)110:3(267)

Smart, G. M., & Jaeggi, M. (1983). Sediment Transport on Steep Slopes. *Mitteilungen Der Versuchsanstalt Fuer Wasserbau, Hydrologie Und Glaziologie, Eidgenossischen Technischen Hochschule, Zurich*, *No. 64*.